Meccanica (2014) 49:1069–1081
DOI 10.1007/s11012-013-9853-1

Analysis for the thermoelastic bending of a functionally graded material cylindrical shell

Hong-Liang Dai · Ting Dai

Received: 23 April 2013 / Accepted: 2 December 2013 / Published online: 6 December 2013

Abstract An analytic study for thermoelastic bending of a functionally graded material (FGM) cylindrical shell subjected to a uniform transverse mechanical load and non-uniform thermal loads is presented. Based on the classical linear shell theory, the equations with the radial deflection and horizontal displacement are derived out. An arbitrary material property of the FGM cylindrical shell is assumed to vary through the thickness of the cylindrical shell, and exact solution of the problem is obtained by using an analytic method. For the FGM cylindrical shell with fixed and simply supported boundary conditions, the effects of mechanical load, thermal load and the power law exponent on the deformation of the FGM cylindrical shell are analyzed and discussed.

H.-L. Dai (✉) · T. Dai
State Key Laboratory of Advanced Design and Manufacturing for Vehicle Body, Hunan University, Changsha 410082, China
e-mail: hldai520@sina.com

H.-L. Dai
Key Laboratory of Manufacture and Test Techniques for Automobile Parts, Ministry of Education, Chongqing University of Technology, Chongqing 400054, China

H.-L. Dai · T. Dai
Department of Engineering Mechanics, College of Mechanical & Vehicle Engineering, Hunan University, Changsha 410082, China

Keywords Functionally graded material · Cylindrical shell · Bending · Thermoelastic

1 Introduction

Cylindrical shell is a kind of broad engineering background shell structure or component. For example, it can be a barrel, and also can be used as a variety of chemical systems and boiler system piping. In many cases, these structures are working in high-temperature gradient environments. FGM are microscopically inhomogeneous materials, by choosing specific manufacturing processing, the property of the produced FGMs may vary from points to points or from layers to layers. Therefore, FGM has been widely applied to such structural components working in high temperature environments.

Many studies for FGM cylindrical structures are available in the literatures, by means of the Bolotin's method, Ng et al. [1] presented a formulation for the dynamic stability analysis of FGM shells under harmonic axial loading. Based on the first order shell theory, Sofiyev et al. [2, 3] studied the dynamic stability of FGM cylindrical shells subjected to external pressure and moving loads. Zhu et al. [4] presented a three-dimensional theoretical analysis of the dynamic instability region of FGPM cylindrical shells. Applying with the general analytical expressions of natural frequency and mode-shape solutions given by

functional variation and characteristic value analysis, Cao and Wang [5] gave free vibration analysis of FGM cylindrical shells with holes. Embedding isotropic FGM cylindrical shell in a boundless fluid-saturated porous elastic medium, Hasheminejad and Rajabi [6] investigated the two-dimensional dynamic interaction of progressive plane seismic waves. By using the method of power series expansion of continuous displacement components, Matsunaga [7] presented a two-dimensional higher-order deformation theory for vibration and buckling problems of FGM cylindrical shells. Based on the first-order shear deformation theory, the Hamilton's principle and the Maxwell equation, Sheng and Wang [8] presented the coupling equations to govern the electric potential and displacements of FGM cylindrical shells with surface-bonded PZT piezoelectric layer subjected to moving loads. Pradhan et al. [9] presented investigation of the vibration of a FGM cylindrical shell made up of stainless steel and zirconia. By using the power series method, Vel [10] obtained exact elasticity solution for the vibration of FGM anisotropic cylindrical shells. Huang et al. [11] investigated buckling behaviors of FGM cylindrical shells subjected to pure bending load. An analytic solution to the axisymmetric problem of a long, radially polarized, FGM hollow cylinder rotating about its axis at a constant angular velocity was given by Dai et al. [12]. Asemi et al. [13] considered a thick short length FGM hollow cylinder under internal impact loading. Using the Galerkin method, Najafov et al. [14] investigated the torsional vibration and stability problems of FGM orthotropic cylindrical shells in the elastic medium. Based on the generalized differential quadrature method, Tornabene and Viola [15] presented static analysis of FGM doubly-curved shells and panels of revolution.

For the thermal problem of FGM cylindrical structures, Jabbari et al. [16–18] investigated analytical methods for analysis of uncoupled thermoelasticity on FGM hollow cylinder. Haddadpour et al. [19] investigated free vibration analysis of FGM cylindrical shells including thermal effects. An algorithm for investigation of nonlinear systems by the transfinite element method was presented by Azadi and Shariyat [20]. Dai and Zheng [21] studied buckling and post-buckling behaviors of a laminated FGM cylindrical shell with the piezoelectric fiber reinforced composite actuators subjected to thermal and axial compressed loads. By means of the Meshless Local Petrov-Galerkin Method, Sladek et al. [22] presented the thermal analysis of Reissner-Mindlin shallow shells with FGM properties, Hosseini et al. [23, 24] investigated the coupled thermoelasticity analysis and thermoelastic wave propagation analysis for FGM thick hollow cylinders. Shen et al. [25–32] presented series of post-buckling analysis and nonlinear vibration study for cylindrical shells in thermal environments. Based on the Donnell's shell theory, Wu et al. [33] discussed the problems of thermal buckling in axial direction of FGM cylindrical shells. Pelletier and Vel [34] obtained an exact solution of FGM cylindrical shells by using the power series expansion and semi-inverse method, and focused on analyzing the volume fraction of different material's effects on the results. Zhang et al. [35] presented the nonlinear dynamical analysis of a clamped-clamped FGM cylindrical shell subjected to an external excitation and uniform temperature change. Shariyat [36, 37] investigated dynamic buckling of imperfect FGM cylindrical shells with integrated surface-bonded sensor and actuator layers subjected to some complex combinations of thermo-electro-mechanical loads. Santos et al. [38] developed a semi-analytical finite element model for the analysis of FGM cylindrical shells under thermal shock. Based on a modified version of Sander's nonlinear shell theory, Zhao et al. [39, 40] studied nonlinear problem of FGM cylindrical shells under mechanical and thermal loading. Based on the first-order shear deformation theory, Sheng and Wang [41, 42] gave a approximate solution for laminated FGM cylindrical shells under thermal shock and mechanical loads by utilizing Hamilton's principle. Based on the nonlinear large deflection theory of cylindrical shells, Huang and Han [43] dealt with the nonlinear buckling problem of FGM cylindrical shells under torsion load by using the energy method and the nonlinear strain-displacement relations of large deformation. Alibeigloo [44] studied infinitesimal axisymmetric deformations of a FGM cylindrical shell with piezoelectric layers perfectly bonded to its inner and outer surfaces which subjected to thermo-electro-mechanical loads. Based on the first order shear deformation theory of shells, Malekzadeh et al. [45–47] presented the free vibration analysis of rotating functionally graded cylindrical shells subjected to thermal environment. However, in our views, analysis for the thermoelastic bending of a functionally graded material

cylindrical shell has not been found in the literature.

Based on the classical linear shell theory, this paper has derived out the equations with the radial deflection and horizontal displacement, and studies on the deformation of a FGM cylindrical shell subjected to a uniform transverse mechanical load and non-uniform thermal loads. According to the FGM cylindrical shell with fixed and simply supported boundary conditions, the effects of loads and material parameters on the deformation of the FGM cylindrical shell are discussed. To our knowledge, however, analytical study on the thermoelastic bending behavior of a FGM cylindrical shell has not been found in the literatures.

2 Formulation of the problem

Consider a FGM cylindrical shell subjected to a uniform transverse mechanical load q and thermal load $T(z)$, and its mean radius of a, the length L and thickness h as shown in Fig. 1. The Cartesian coordinate system (x, y, z) is set on the mid-plane $(z = 0)$ of the FGM cylindrical shell, where x and y denotes the axial and circumferential directions of the middle surface of the FGM cylindrical shell, respectively.

2.1 Material properties of FGM

The FGM cylindrical shell is composed of metal and ceramic and the composition varies from the top to the bottom surfaces, i.e. the top surface $(z = h/2)$ of the cylindrical shell is metal-rich whereas the bottom surface $(z = -h/2)$ is ceramic-rich. In this way, an arbitrary material property P (e.g., Young's modulus E, thermal expansion coefficient α and thermal conductivity K) of the FGM cylindrical shell is assumed to vary through the thickness of the shell. FGM's material properties P are related not only to the material properties of the constituents, but also to their volume fractions V_1 and V_2, therefore, one has

$$P(z) = P_1 V_1 + P_2 V_2, \quad V_1 + V_2 = 1 \tag{1}$$

where P_1 and P_2 denote properties of the top and bottom surfaces of the FGM cylindrical shell.

Assuming V_1 follows a simple power law distribution as

$$V_1 = \left(\frac{h - 2z}{2h}\right)^n \tag{2}$$

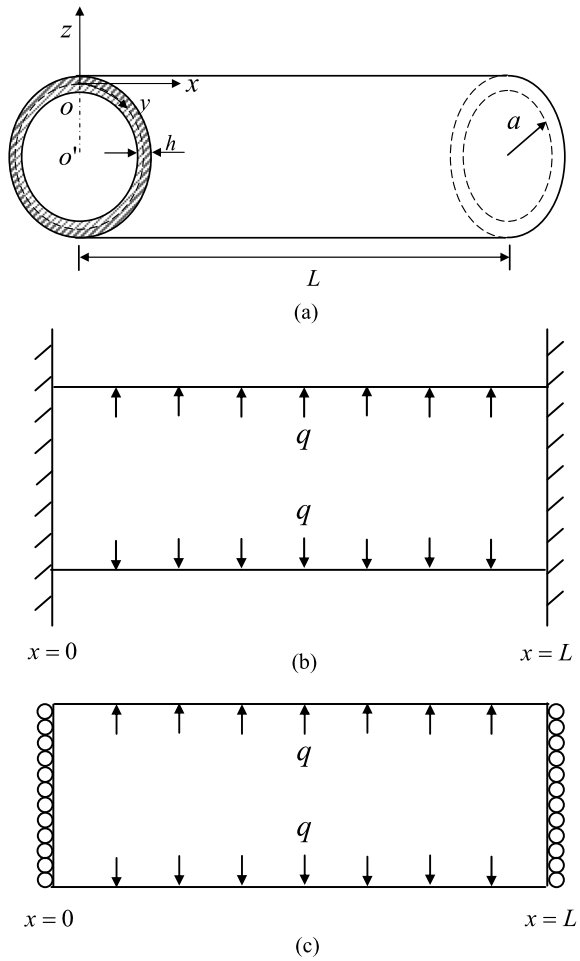

Fig. 1 (**a**) The geometry of a FGM cylindrical shell; (**b**) Fixed of both ends; (**c**) Simply supported of both ends

where n $(0 < n < \infty)$ is the volume fraction of ceramic, and n represents the inhomogeneity of FGMs, and it degenerated into metal at $n = 0$, when $n \to \infty$, it becomes ceramic.

Using Eq. (3), the material properties of FGMs are written as

$$P(z) = (P_1 - P_2)(0.5 - z/h)^n + P_2 \tag{3}$$

where FGM's properties vary smoothly from P_1 $(z = h/2)$ to P_2 $(z = -h/2)$ through the thickness according to n.

2.2 Basic equations

According to the symmetric geometry of the FGM cylindrical shell, one has

$$\varepsilon_x = \varepsilon_x^0 + z k_x^0, \qquad \varepsilon_\theta = \varepsilon_\theta^0 + z k_\theta^0, \qquad \varepsilon_z = 0 \tag{4}$$

where

$$\varepsilon_x^0 = \frac{\partial u}{\partial x}, \qquad \varepsilon_\theta^0 = -\frac{w}{a},$$
$$k_x^0 = \frac{\partial^2 w}{\partial x^2}, \qquad k_\theta^0 = \frac{w}{a^2} \tag{5}$$

where u, v, w are the displacements along x, y and z axes, respectively, ε_x^0 and ε_θ^0 are, respectively, strain components of x and y direction on the middle surface, k_x^0 and k_θ^0 are corresponding to curvature change.

The linear thermoelastic constitutive relations of the FGM cylindrical shell are

$$\sigma_x = \frac{E(z)}{1-v^2}(\varepsilon_x + v\varepsilon_\theta) - \frac{E(z)}{1-v}\alpha(z)T(z) \tag{6a}$$

$$\sigma_\theta = \frac{E(z)}{1-v^2}(\varepsilon_\theta + v\varepsilon_x) - \frac{E(z)}{1-v}\alpha(z)T(z) \tag{6b}$$

where σ_x, σ_θ are stress components of the x and y direction respectively, usually the material's Poisson ratio v changes along the thickness direction is small, for simplicity, assuming v to be a constant.

Consider the FGM cylindrical shell's axial-symmetry behavior, the balance equations are

$$a\frac{\partial Q_x}{\partial x} - N_\theta - aq = 0 \tag{7a}$$

$$a\frac{\partial N_x}{\partial x} = 0 \tag{7b}$$

$$a\frac{\partial M_x}{\partial x} + aQ_x = 0 \tag{7c}$$

where Q_x is transverse shear, q is mechanical load, membrane force N_θ, N_x and moment M_x are defined as

$$N_x = \int_{-h/2}^{h/2} \sigma_x \left(1 + \frac{z}{a}\right) \mathrm{d}z \tag{8a}$$

$$N_\theta = \int_{-h/2}^{h/2} \sigma_\theta \mathrm{d}z \tag{8b}$$

$$M_x = -\int_{-h/2}^{h/2} \sigma_x z \left(1 + \frac{z}{a}\right) \mathrm{d}z \tag{8c}$$

Assume that the temperature rise occurs in the thickness direction only, the temperature field solving the following one-dimensional steady conduction equations is

$$\frac{\mathrm{d}}{\mathrm{d}z}\left(K(z)\frac{\mathrm{d}T(z)}{\mathrm{d}z}\right) = 0 \tag{9}$$

The corresponding thermal boundary conditions are

$$T\left(-\frac{h}{2}\right) = T_1, \qquad T\left(\frac{h}{2}\right) = T_2 \tag{10}$$

where T_1 and T_2 are the inner surface temperature and outer surface temperature of the FGM cylindrical shell, and the analytic solution is written as

$$T(z) = T_1\left[1 + (T_r - 1)\frac{\int_{-h/2}^{z} \frac{1}{K(z)}\mathrm{d}z}{\int_{-h/2}^{h/2} \frac{1}{K(z)}\mathrm{d}z}\right] \tag{11}$$

where

$$T_r = \frac{T_1}{T_2} \tag{12}$$

Substituting Eqs. (4)–(6a), (6b) and (11) into Eqs. (8a)–(8c), yields

$$N_x = A_{10}\left(\varepsilon_z^0 + v\varepsilon_\theta^0\right) + B_{10}\left(k_z^0 + vk_\theta^0\right) - \Gamma_1^* \tag{13a}$$

$$N_\theta = A_{20}\left(\varepsilon_\theta^0 + v\varepsilon_z^0\right) + B_{20}\left(k_\theta^0 + vk_z^0\right) - \Gamma_1 \tag{13b}$$

$$M_x = A_{30}\left(\varepsilon_z^0 + v\varepsilon_\theta^0\right) + B_{30}\left(k_z^0 + vk_\theta^0\right) - \Gamma_2^* \tag{13c}$$

where A_{i0}, B_{i0}, Γ_1^*, Γ_1 and Γ_2^* are shown in Appendix.

3 Solution of the problem

Here, by means of the hybrid method of unknown base quantity (u and w) to solve this problem, utilizing Eqs. (7a)–(7c) to eliminate Q_x, yields

$$a\frac{\partial^2 M_x}{\partial z^2} + N_\theta + aq = 0 \tag{14a}$$

$$\frac{\partial N_x}{\partial x} = 0 \tag{14b}$$

Substituting Eqs. (5) and (13a)–(13c) into Eqs. (14a), (14b), yields

$$aA_{30}\frac{\partial^3 u}{\partial x^3} + A_{20}v\frac{\partial u}{\partial x} + aB_{30}\frac{\partial^4 w}{\partial x^4} + \left(B_{20} - A_{30} + \frac{B_{30}}{a}\right)v\frac{\partial^2 w}{\partial x^2} + \frac{B_{20} - aA_{20}}{a^2}w = \Gamma_1 - aq \tag{15}$$

$$A_{10}\frac{\partial^2 u}{\partial x^2} + \frac{v(B_{10} - aA_{10})}{a^2}\frac{\partial w}{\partial x} + B_{10}\frac{\partial^3 w}{\partial x^3} = 0 \tag{16}$$

Utilizing Eqs. (15) and (16), one gets

$$G_1\frac{\partial^4 w}{\partial x^4} + G_2\frac{\partial^2 w}{\partial x^2} + G_3 w = Q \tag{17}$$

where

$$G_1 = \frac{-A_{30}B_{10}a}{A_{10}} + aB_{30} \tag{18a}$$

$$G_2 = \frac{-A_{30}(B_{10} - aA_{10})v}{A_{10}a} - \frac{A_{20}B_{10}}{A_{10}}$$

$$+\left(B_{20}-A_{30}+\frac{B_{30}}{a}\right) \tag{18b}$$

$$G_3=-\frac{A_{20}(B_{10}-aA_{10})v}{A_{10}}+\frac{B_{20}-aA_{20}}{a^2} \tag{18c}$$

$$Q=\Gamma_1-aq-\frac{A_{20}k_1v}{A_{10}} \tag{18d}$$

$$A_{10}\frac{\partial u}{\partial z}+\frac{v(B_{10}-aA_{10})}{a^2}w+B_{10}\frac{\partial^2 w}{\partial x^2}=k_1 \tag{18e}$$

where k_1 is an integration constant, which is determined by the boundary conditions.

The general solution to Eq. (17) is

$$w=C_1e^{D_1x}+C_2e^{D_2x}+C_3e^{D_3x}+C_4e^{D_4x}+\frac{Q}{G_3} \tag{19}$$

where C_i $(i=1,2,3,4)$ are unknown constants, and

$$\begin{aligned}
D_1&=\sqrt{\frac{-G_2-\sqrt{G_2^2-4G_1G_3}}{2G_1}},\\
D_2&=-\sqrt{\frac{-G_2-\sqrt{G_2^2-4G_1G_3}}{2G_1}},\\
D_3&=\sqrt{\frac{G_2+\sqrt{G_2^2-4G_1G_3}}{2G_1}},\\
D_4&=-\sqrt{\frac{G_2+\sqrt{G_2^2-4G_1G_3}}{2G_1}}
\end{aligned} \tag{20}$$

Then, substituting the obtained w into Eq. (18e), integrate both sides of the equation, yields

$$u=\frac{k_1}{A_{10}}x+\zeta_1e^{D_1x}+\zeta_2e^{D_2x}+\zeta_3e^{Dx}+\zeta_4e^{D_4x}+k_2 \tag{21}$$

where k_1 and k_2 are unknown constants, and

$$\begin{aligned}
\zeta_1&=\frac{-B_{10}C_1D_1}{A_{10}}-\frac{(B_{10}-aA_{10})C_1}{a^2D_1},\\
\zeta_2&=\frac{-B_{10}C_2D_2}{A_{10}}-\frac{(B_{10}-aA_{10})C_2}{a^2D_2}\\
\zeta_3&=\frac{-B_{10}C_3D_3}{A_{10}}-\frac{(B_{10}-aA_{10})C_3}{a^2D_3},\\
\zeta_4&=\frac{-B_{10}C_4D_4}{A_{10}}-\frac{(B_{10}-aA_{10})C_4}{a^2D_4}
\end{aligned} \tag{22}$$

By means of Eq. (21), the expressions of ε_x, ε_θ, σ_x, σ_θ, N_x, N_θ and M_x are shown as follows:

$$\begin{aligned}
\varepsilon_x=&\frac{k_1}{A_{10}}+\frac{Q}{a^2G_3}z+(\zeta_1D_1+C_1D_1^2z)e^{D_1x}\\
&+(\zeta_2D_2+C_2D_2^2z)e^{D_2x}+(\zeta_3D_3+C_3D_3^3z)e^{D_3x}\\
&+(\zeta_4D_4+C_4D_4^2z)e^{D_4x}
\end{aligned} \tag{23}$$

$$\begin{aligned}
\varepsilon_\theta=&\left(\frac{1}{a^2}z-\frac{1}{a}\right)\left[\frac{Q}{G_3}+C_1e^{D_1x}+C_2e^{D_2x}\right.\\
&\left.+C_3e^{D_3x}+C_4e^{D_4x}\right]
\end{aligned} \tag{24}$$

$$\begin{aligned}
\sigma_x=&\frac{A_{10}E_2}{1-v^2}\left(1+(E_r-1)\left(\frac{h-2z}{2h}\right)^n\right)\\
&\times\left(\frac{k_1}{A_{10}}-\frac{Q}{aG_3}\right)v+\sum_{i=1}^{4}\left(\zeta_iD_i-\frac{C_i}{a}v\right)e^{D_ix}\\
&-\frac{E_2\alpha_1T_1}{1-v}\left[1+(E_r-1)\left(\frac{h-2z}{2h}\right)^n\right]\\
&\times\left[\alpha_r+(1-\alpha_r)\left(\frac{h-2z}{2h}\right)^n\right]\\
&\times\left[1+(T_r-1)\frac{\Psi_a}{\Psi_b}\right]
\end{aligned} \tag{25}$$

$$\begin{aligned}
\sigma_\theta=&\frac{A_{10}E_2}{1-v^2}\left(1+(E_r-1)\left(\frac{h-2z}{2h}\right)^n\right)\\
&\times\left(\frac{k_1}{A_{10}}v-\frac{Q}{aG_3}\right)+\sum_{i=1}^{4}\left(\zeta_iD_iv-\frac{C_i}{a}\right)e^{D_ix}\\
&-\frac{E_2\alpha_1T_1}{1-v}\left[1+(E_r-1)\left(\frac{h-2z}{2h}\right)^n\right]\\
&\times\left[\alpha_r+(1-\alpha_r)\left(\frac{h-2z}{2h}\right)^n\right]\\
&\times\left[1+(T_r-1)\frac{\Psi_a}{\Psi_b}\right]
\end{aligned} \tag{26}$$

$$\begin{aligned}
N_x=&A_{10}\left(\frac{k_1}{A_{10}}-\frac{Q}{aG_3}v+\sum_{i=1}^{4}\left(\zeta_iD_i-\frac{C_i}{a}v\right)e^{D_ix}\right)\\
&+B_{10}\left(\frac{Q}{aG_3}v+\sum_{i=1}^{4}C_i\left(D_i^2+\frac{1}{a^2}v\right)e^{D_ix}\right)\\
&-\Gamma_1^*
\end{aligned} \tag{27}$$

$$\begin{aligned}
N_\theta=&A_{20}\left(\frac{k_1}{A_{10}}v-\frac{Q}{aG_3}+\sum_{i=1}^{4}\left(\zeta_iD_iv-\frac{C_i}{a}\right)e^{D_ix}\right)\\
&+B_{20}\left(\frac{Q}{aG_3}v+\sum_{i=1}^{4}C_i\left(D_i^2v+\frac{1}{a^2}\right)e^{D_ix}\right)\\
&-\Gamma_1
\end{aligned} \tag{28}$$

$$M_x = A_{30}\left(\frac{k_1}{A_{10}} - \frac{Q}{aG_3}v + \sum_{i=1}^{4}\left(\zeta_i D_i - \frac{C_i}{a}v\right)e^{D_i x}\right) + B_{30}\left(\frac{Q}{aG_3}v + \sum_{i=1}^{4} C_i\left(D_i^2 + \frac{1}{a^2}v\right)e^{D_i x}\right) - \Gamma_3^* \tag{29}$$

where C_1, C_2, C_3, C_4, k_1 and k_2 are unknown constants, which are determined by the boundary conditions.

4 Numerical results and discussions

Considering a FGM cylindrical shell under uniform transverse mechanical load and non-uniform thermal loads, analytical solution for the thermoelastic-static deformation response of the FGM cylindrical shell is given.

Two kinds of boundary conditions can be expressed as:

(1) The fixed boundary condition (see Fig. 1(b))

$$w = u = \frac{\mathrm{d}w}{\mathrm{d}x} = 0, \quad \text{at } x = 0, L \tag{30a}$$

(2) The simply supported boundary condition (see Fig. 1(c))

$$w = u = 0, \qquad M_x = 0, \quad \text{at } x = 0, L \tag{30b}$$

Utilizing boundary condition Eq. (30a) or Eq. (30b), and the unknown constants C_1, C_2, C_3, C_4, k_1 and k_2 can be determined.

In all numerical calculations, the FGM cylindrical shell is made from a mixture of ceramic and metal, which are taken as a metallic material Aluminum and a ceramic material Zirconia, denoted as (ZrO_2/Al), the following material constants for the FGM cylindrical shell are adopted (Zhang et al. [35]; Ma and Wang [48]).

ZrO_2: $E_2 = 151$ GPa, $\alpha_2 = 10 \times 10^{-6}/\,^\circ$C,

$K_2 = 2.09$ W/(m °C), $v = 0.30$

Al: $E_1 = 70$ GPa, $\alpha_1 = 23 \times 10^{-6}/^\circ$C,

$K_2 = 2.04$ W/(m °C), $v = 0.30$

Example 1 In this example, geometry of a FGM cylindrical shell is taken as: $a = 1$ m, $L = 4$ m and $h = 2$ cm. Investigation on variations of the radial deflection of the fixed and simply supported FGM cylindrical shell subjected to a uniform transverse mechanical load and non-uniform thermal loads.

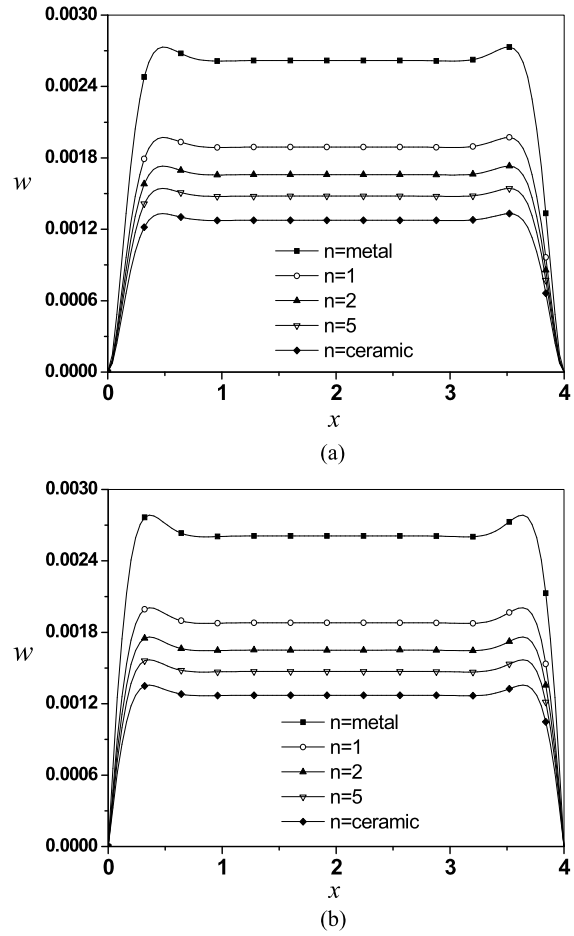

Fig. 2 Radial deflections of the fixed FGM cylindrical shell subjected to mechanical load $q = 1$ MPa, when $T_1 = 0$ °C and $T_r = 0$, (**a**) Fixed of both ends; (**b**) Simply supported of both ends

Case 1 The fixed and simply supported FGM cylindrical shell subjected to mechanical and thermal loads are expressed as

$$q = 1 \text{ MPa}, \qquad T_1 = 0\,^\circ\text{C} \quad \text{and} \quad T_r = 0 \tag{31}$$

Figures 2(a) and 2(b) show radial deflection of the FGM cylindrical shell subjected only to a mechanic load, with different volume fraction index n, at the fixed and simply supported boundary conditions, respectively. From the curves of Fig. 2(a), it is seen easily that the maximum point of radial deflection of the fixed FGM cylindrical shell is not at the center of the FGM cylindrical shell, but near to the end about 0.4 m. It is also seen from the curves that the radial deflection of the fixed FGM cylindrical shell decreases as the volume fraction index n increases when subjected only to

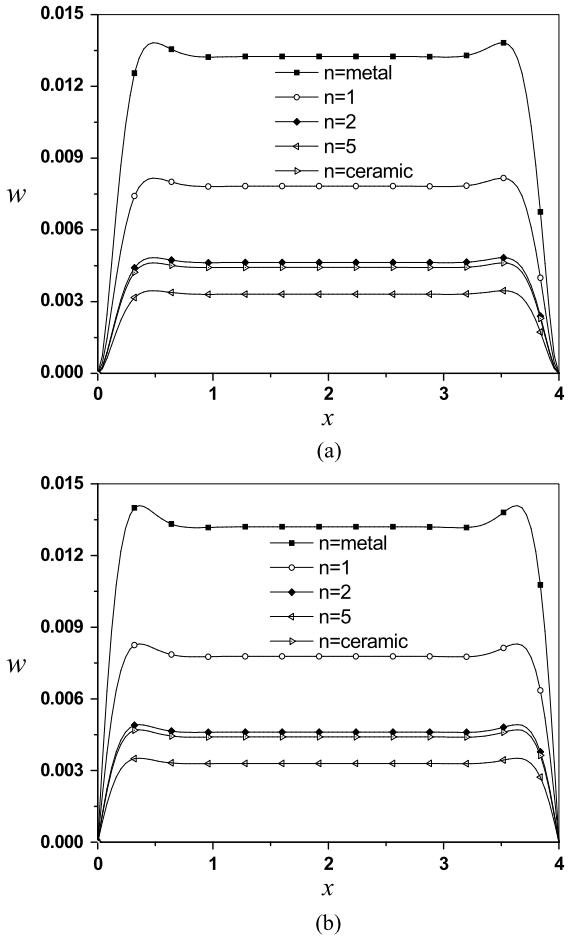

Fig. 3 Radial deflections of the simply supported FGM cylindrical shell subjected to mechanical load $q = 1$ MPa and thermal loads $T_1 = 40$ °C, $T_r = 10$, (**a**) Fixed of both ends; (**b**) Simply supported of both ends

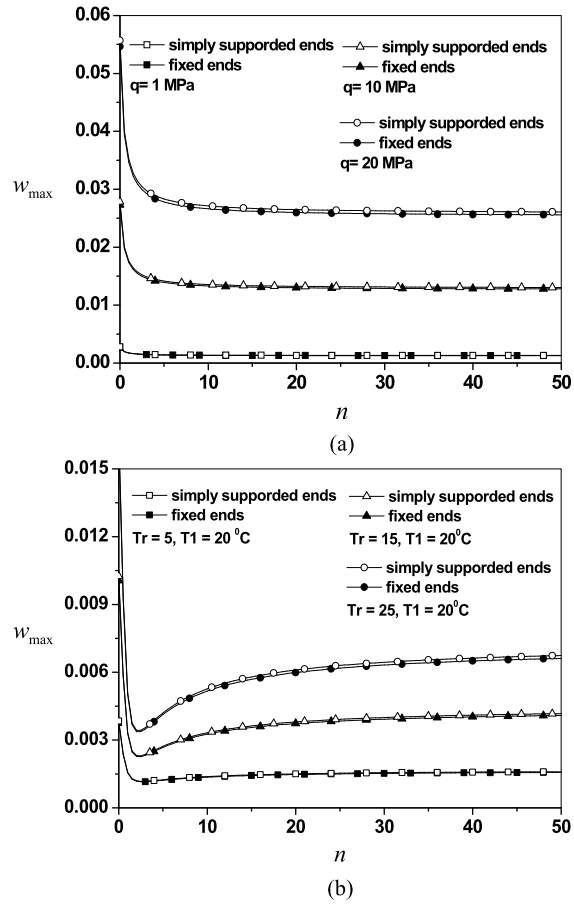

Fig. 4 Variation of the maximal radial deflections for the FGM cylindrical shell with the increasing of n, (**a**) Subjected to mechanical load q, when $T_1 = 0$ °C and $T_r = 0$; (**b**) Subjected to thermal load T_r, when $q = 1$ MPa and $T_1 = 20$ °C

mechanical load. Comparing Fig. 2(a) with Fig. 2(b), the change trend of radial deflection is similar at the fixed and simply supported boundary conditions, then the maximum point of radial deflection of the simply supported FGM cylindrical shell is near to the end about 0.3 m.

Case 2 The fixed and simply supported FGM cylindrical shell subjected to uniform transverse mechanical load and non-uniform thermal loads are expressed as

$$q = 1 \text{ MPa}, \qquad T_1 = 40\,^{\circ}\text{C} \quad \text{and} \quad T_r = 10 \qquad (32)$$

Figures 3(a) and 3(b) show various curves of radial deflection w of the FGM cylindrical shell subjected to mechanical and thermal loads with different volume fraction index n, at the fixed and simply supported boundary conditions, respectively. From the Figs. 3(a) and 3(b), it is easily seen that the radial deflection of the FGM cylindrical shell is similar to the fixed shell in Fig. 2.

Case 3 Investigation on the maximum value of radial deflection of the fixed and simply supported FGM cylindrical shell subjected to different mechanical loads and thermal loads.

Figure 4(a) shows comparison of maximum radial deflection ($W_{\max}$) of the FGM cylindrical shell versus different volume fraction index n, subjected to different mechanic loads, at the fixed and simply supported boundary conditions. From Fig. 4(a), under the same conditions, it can be seen that the $W_{\max}$ of the simply supported FGM cylinder shell is greater than that

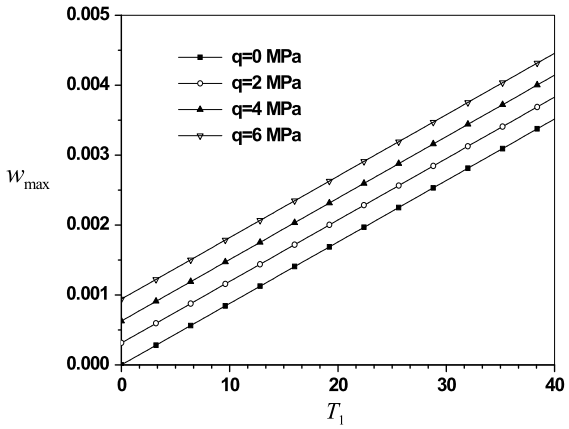

Fig. 5 Variation of the maximal radial deflections for the fixed FGM cylindrical shell with the increasing of T_1, where $q = 0, 2, 4, 6$ MPa, $T_r = 10$ and $n = 2$

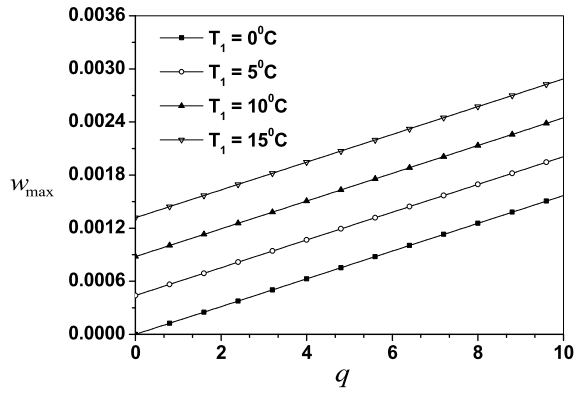

Fig. 6 Variation of the maximal radial deflections for the fixed FGM cylindrical shell with the increasing of q, where $T_1 = 0, 5, 10, 15(°C)$, $T_r = 10$ and $n = 2$

of the fixed FGM cylindrical shell. It can also be seen from the Fig. 4(a) that the W_{max} is decreases as the n increases.

Figure 4(b) shows comparison of the W_{max} of the FGM cylindrical shell versus different volume fraction indexes n, subjected to different temperature loads, at the fixed and simply supported boundary conditions. It is easily seen from Fig. 4(b) that the W_{max} of the simply supported shell is greater than that of the fixed FGM cylindrical shell at the same conditions. It is also seen from the Fig. 4(b) that the change of W_{max} is non-monotonically as n increases, W_{max} decreases rapidly as n increases at $0 \leq n \leq 2.2$, and W_{max} increases as n increases at $n > 2.2$, the change trend is more and more slowly. From Figs. 4(a) and 4(b), it is seen easily that the W_{max} of the fixed and simply supported FGM cylindrical shell increases as the load increases.

Figures 5 and 6 show the W_{max} of the fixed FGM cylindrical shell subjected to different mechanical loads and thermal loads, respectively. From the Figs. 5 and 6, it is seen easily that the increasing of the W_{max} is proportional with both the mechanical and thermal loads increase.

Example 2 In this example, investigation on variations of axial and circumferential stresses of the fixed and simply supported FGM cylindrical subjected to a uniform transverse mechanical load and non-uniform thermal loads.

Figures 7 and 8 show, respectively, axial and circumferential stresses of the fixed FGM cylindrical shell subjected to mechanical load with the change of thickness h at $x = 0, 0.2, 0.6$. From Figs. 7(a–c), it is seen easily that the axial stress has a similar change in trend as the variation of x except at $x = 0$. From the Figs. 7 and 8, when $n = 0$, that is, the FGM degraded into metallic material, it is seen easily from the curves that the axial and circumferential stresses are linear with the change of thickness of the fixed FGM cylindrical shell.

Example 3 In this example, introduce aspect ratio $k = a/h$, where $a = 1$ m and $n = 1$. According to different aspect ratio, investigation on variations of the radial deflection, axial and circumferential stresses along the x direction of the fixed FGM cylindrical subjected to a uniform transverse mechanical load and non-uniform thermal loads.

Figures 9, 10, and 11 show, respectively, radial deflection, axial stress and circumferential stress of the fixed FGM cylindrical shell, subjected only to mechanical load ($q = 1$ MPa, $T_1 = 0$ °C and $T_r = 0$), along the x direction with different aspect ratio k. From Fig. 9, one knows, the value of radial deflection of the fixed FGM cylindrical shell subjected only to mechanical load is positive, and it is creases as the increasing of aspect ratio k. It is seen easily from Fig. 10 that the change of axial stress along the x direction is creases with the increasing of aspect ratio k. From Fig. 11, one knows, the change trend of circumferential stress is similar as the change trend of axial stress.

Figure 12 shows radial deflection of the fixed FGM cylindrical shell subjected only to thermal load ($T_1 = 15$ °C, $T_r = 10$ and $q = 0$) along the x direction with different aspect ratio k. It is seen easily from Fig. 12

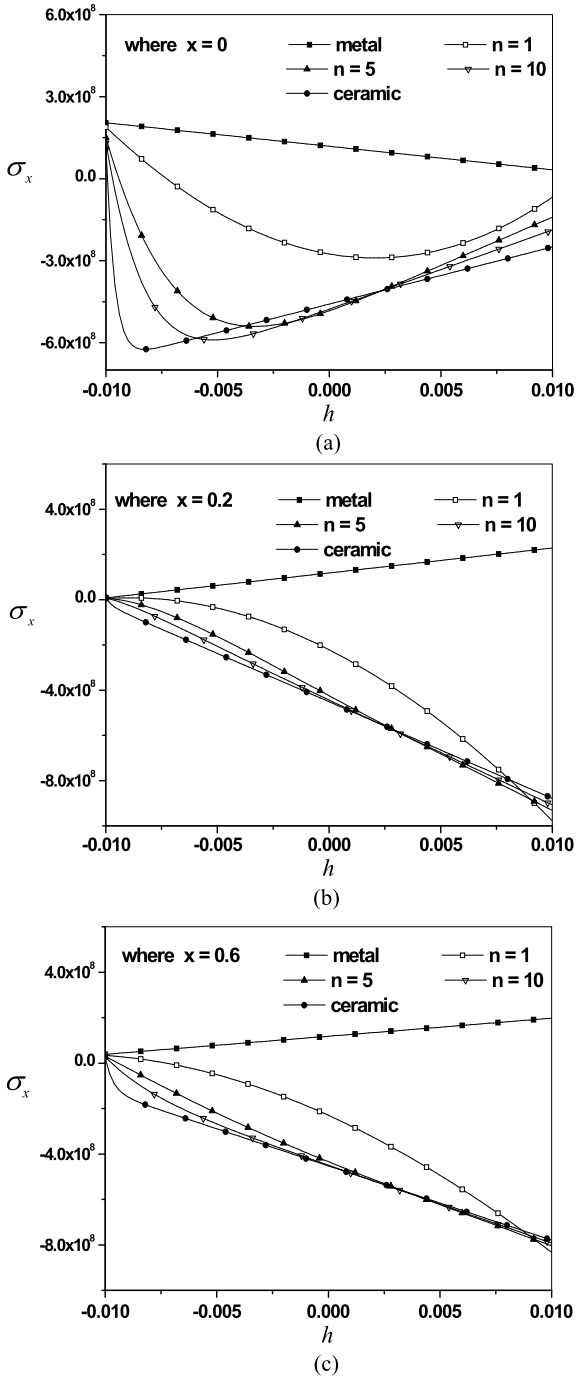

Fig. 7 Axial stresses of the FGM cylindrical shell subjected to mechanical load $q = 1$ MPa with the change of thickness h, where (**a**) $x = 0$; (**b**) $x = 0.2$; (**c**) $x = 0.6$

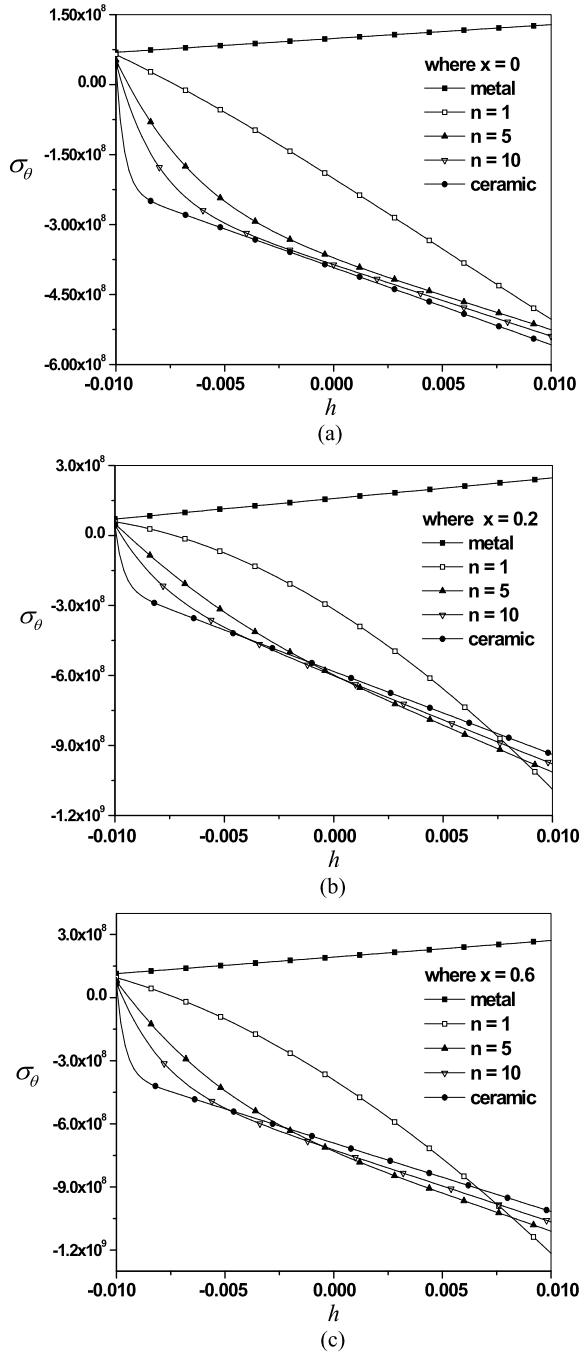

Fig. 8 Circumferential stresses of the FGM cylindrical shell subjected to mechanical load $q = 1$ MPa with the change of thickness h, where (**a**) $x = 0$; (**b**) $x = 0.2$; (**c**) $x = 0.6$

that the value of radial deflection of the fixed FGM cylindrical shell is negative, the peak value of radial deflection is almost the same, and the location of the peak radial deflection is affected by aspect ratio k. Figures 13 and 14 show axial stress and circumferential stress of the fixed FGM cylindrical shell subjected

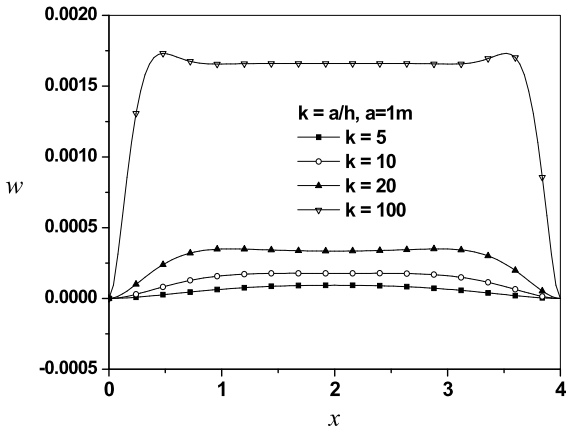

Fig. 9 Radial deflections of the fixed FGM cylindrical shell along the x direction with different aspect ratios, where $n = 1$, $q = 1$ MPa, $T_1 = 0$ °C and $T_r = 0$

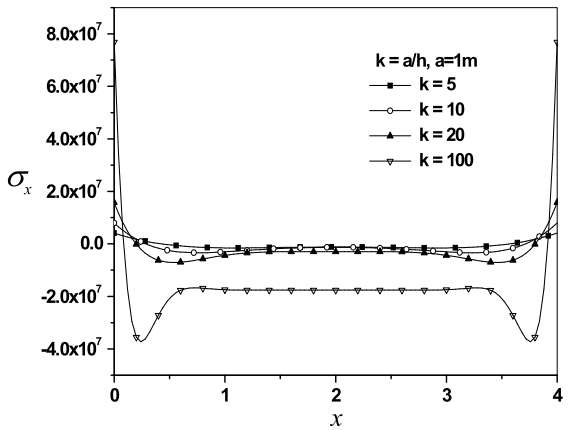

Fig. 10 Axial stresses of the fixed FGM cylindrical shell along the x direction with different aspect ratios, where $n = 1$, $q = 1$ MPa, $T_1 = 0$ °C and $T_r = 0$

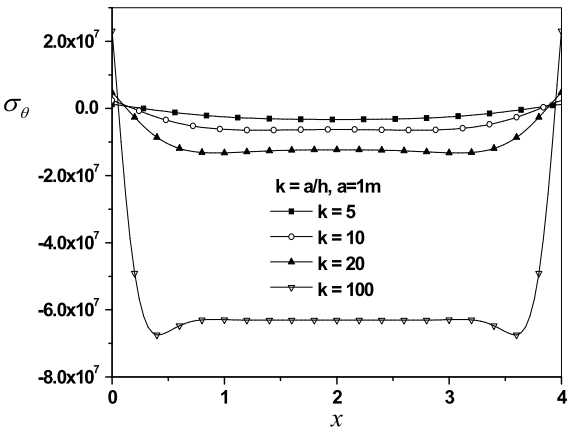

Fig. 11 Circumferential stresses of the fixed FGM cylindrical shell along the x direction with different aspect ratios, where $n = 1$, $q = 1$ MPa, $T_1 = 0$ °C and $T_r = 0$

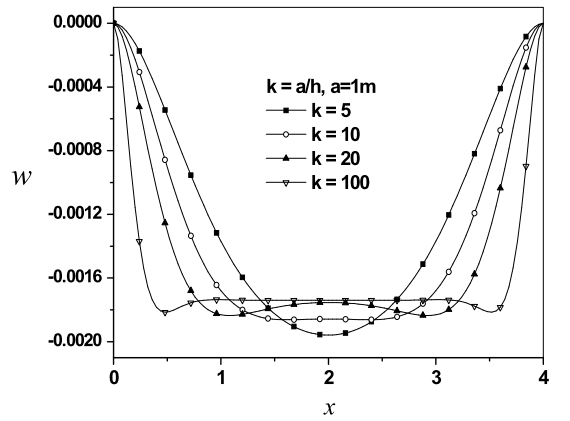

Fig. 12 Radial deflections of the fixed FGM cylindrical shell along the x direction with different aspect ratios, where $n = 1$, $q = 0$, $T_1 = 15$ °C and $T_r = 10$

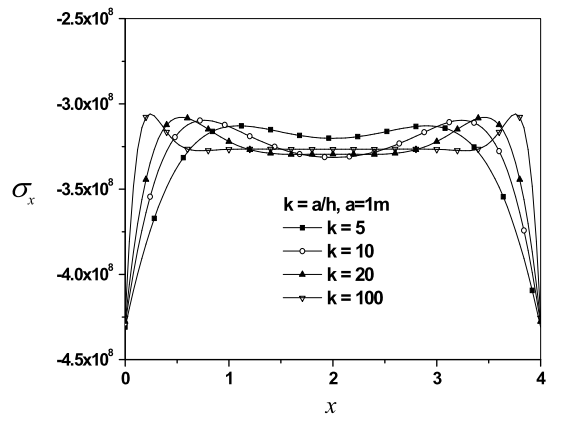

Fig. 13 Axial stresses of the fixed FGM cylindrical shell along the x direction with different aspect ratios, where $n = 1$, $q = 0$, $T_1 = 15$ °C and $T_r = 10$

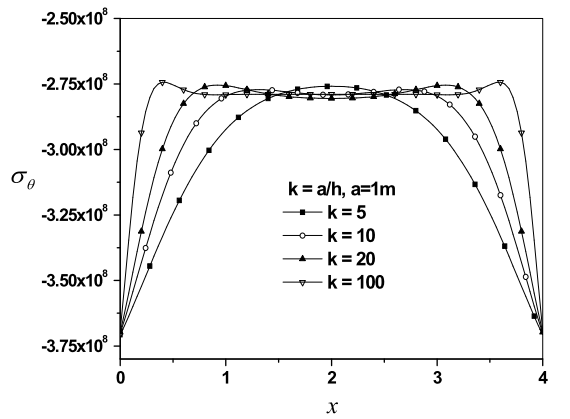

Fig. 14 Circumferential stresses of the fixed FGM cylindrical shell along the x direction with different aspect ratios, where $n = 1$, $q = 0$, $T_1 = 15$ °C and $T_r = 10$

only to thermal load along the x direction with different aspect ratio k, respectively. It is seen easily from Figs. 13 and 14 that the peak values of stresses are almost the same, and the location of the peak stresses are affected by aspect ratio k.

5 Conclusions

Based on classical linear shell theory, an analytic solution for deformation of a FGM cylindrical shell subjected to a uniform transverse mechanical load and non-uniform thermal loads is presented. A few conclusions can be drawn as follows:

(1) Numerical results show that the radial deflection does not occur in the middle but near to both ends of the fixed or simply supported FGM cylindrical shell when the shell subjected to a uniform transverse mechanical load and non-uniform thermal loads.
(2) The power law exponent, mechanical load, thermal load and aspect ratios have a great effect on axial stress, circumferential stress and the radial deflection of the fixed or simply supported FGM cylindrical shell.
(3) By selecting a proper value of the power law exponent, aspect ratios, suitable load and boundary condition, it is possible for engineering to design the FGM cylindrical shell that can meet some special requirements.

Acknowledgements The authors wish to thank reviewers for their valuable comments and the research is supported by the National Natural Science Foundation of China (11372105), New Century Excellent Talents Program in University (NCET-13-0184), Key Laboratory of Manufacture and Test Techniques for Automobile Parts, Ministry of Education (2012), Hunan Provincial Natural Science Foundation for Creative Research Groups of China (12JJ7001), and the central colleges of basic scientific research and operational costs (funded by the Hunan University).

Appendix

$$
\begin{aligned}
&A_{10} = \Theta_{10} + \Theta_{12}, \qquad B_{10} = \Theta_{11} + \Theta_{13},\\
&\Gamma_1^* = \Gamma_1 + \tfrac{1}{a}\Gamma_2, \qquad A_{20} = \Theta_{10},\\
&B_{20} = \Theta_{11}, \qquad A_{30} = -a\Theta_{12} - \Theta_{13},\\
&B_{30} = -a\Theta_{13} - \Theta_{14}, \qquad \Gamma_2^* = -\Gamma_2 - \tfrac{1}{a}\Gamma_3
\end{aligned}
\tag{A.1}
$$

$$
\begin{aligned}
\Theta_{10} &= \int_{-h/2}^{h/2} \frac{E_2}{1-v^2}\left(1 + (E_r - 1)\left(\frac{h-2z}{2h}\right)^n\right)\mathrm{d}z\\
\Theta_{11} &= \int_{-h/2}^{h/2} \frac{E_2}{1-v^2}\left(1 + (E_r - 1)\left(\frac{h-2z}{2h}\right)^n\right)z\mathrm{d}z\\
\Theta_{12} &= \frac{1}{a}\int_{-h/2}^{h/2} \frac{E_2}{1-v^2}\left(1 + (E_r - 1)\left(\frac{h-2z}{2h}\right)^n\right)\\
&\quad \times z\mathrm{d}z\\
\Theta_{13} &= \frac{1}{a}\int_{-h/2}^{h/2} \frac{E_2}{1-v^2}\left(1 + (E_r - 1)\left(\frac{h-2z}{2h}\right)^n\right)\\
&\quad \times z^2\mathrm{d}z\\
\Theta_{14} &= \frac{1}{a}\int_{-h/2}^{h/2} \frac{E_2}{1-v^2}\left(1 + (E_r - 1)\left(\frac{h-2z}{2h}\right)^n\right)\\
&\quad \times z^3\mathrm{d}z
\end{aligned}
\tag{A.2}
$$

$$
\begin{aligned}
\Gamma_1 &= \int_{-h/2}^{h/2} \frac{E(z)}{1-v}\alpha(z)T(z)\mathrm{d}z = \Delta_{10} + \Delta_{11} + \Delta_{12}\\
&\quad + \Delta_{13} + \Delta_{14} + \Delta_{15}\\
\Gamma_2 &= \int_{-h/2}^{h/2} \frac{E(z)}{1-v}\alpha(z)T(z)z\mathrm{d}z = \Delta_{20} + \Delta_{21} + \Delta_{22}\\
&\quad + \Delta_{23} + \Delta_{24} + \Delta_{25}\\
\Gamma_3 &= \int_{-h/2}^{h/2} \frac{E_2\alpha_1 T_1}{1-v}\alpha_r z^2\mathrm{d}z = \Delta_{30} + \Delta_{31} + \Delta_{32}\\
&\quad + \Delta_{33} + \Delta_{34} + \Delta_{35}
\end{aligned}
\tag{A.3}
$$

$$
\begin{aligned}
\Delta_{10} &= \int_{-h/2}^{h/2} \frac{E_2\alpha_1 T_1}{1-v}\alpha_r\mathrm{d}z,\\
\Delta_{11} &= \int_{-h/2}^{h/2} \frac{E_2\alpha_1 T_1}{1-v}(1 - 2\alpha_r + \alpha_r E_r)\left(\frac{h-2x}{2h}\right)^n\mathrm{d}x\\
\Delta_{12} &= \int_{-h/2}^{h/2} \frac{E_2\alpha_1 T_1}{1-v}(1-\alpha_r)(E_r - 1)\left(\frac{h-2z}{2h}\right)^{2n}\mathrm{d}z\\
\Delta_{13} &= \int_{-h/2}^{h/2} \frac{E_2\alpha_1 T_1}{1-v}(T_r - 1)\alpha_r\frac{\Psi_a}{\Psi_b}\mathrm{d}z\\
\Delta_{14} &= \int_{-h/2}^{h/2} \frac{E_2\alpha_1 T_1}{1-v}(T_r - 1)(1 - 2\alpha_r\\
&\quad + \alpha_r E_r)\left(\frac{h-2z}{2h}\right)^n\frac{\Psi_a}{\Psi_b}\mathrm{d}z\\
\Delta_{15} &= \int_{-h/2}^{h/2} \frac{E_2\alpha_1 T_1}{1-v}(T_r - 1)(1-\alpha_r)\\
&\quad \times (E_r - 1)\left(\frac{h-2z}{2h}\right)^{2n}\frac{\Psi_a}{\Psi_b}\mathrm{d}z\\
\Delta_{20} &= \int_{-h/2}^{h/2} \frac{E_2\alpha_1 T_1}{1-v}\alpha_r z\mathrm{d}z
\end{aligned}
$$

$$\Delta_{21} = \int_{-h/2}^{h/2} \frac{E_2\alpha_1 T_1}{1-v}(1-2\alpha_r + \alpha_r E_r)\left(\frac{h-2z}{2h}\right)^n z\,\mathrm{d}z$$

$$\Delta_{22} = \int_{-h/2}^{h/2} \frac{E_2\alpha_1 T_1}{1-v}(1-\alpha_r) \times (E_r-1)\left(\frac{h-2x}{2h}\right)^{2n} x\,\mathrm{d}x$$

$$\Delta_{23} = \int_{-h/2}^{h/2} \frac{E_2\alpha_1 T_1}{1-v}(T_r-1)\alpha_r \frac{\Psi_a}{\Psi_b} z\,\mathrm{d}z \qquad (A.4)$$

$$\Delta_{24} = \int_{-h/2}^{h/2} \frac{E_2\alpha_1 T_1}{1-v}(T_r-1)(1-2\alpha_r+\alpha_r E_r) \times \left(\frac{h-2z}{2h}\right)^n \frac{\Psi_a}{\Psi_b} z\,\mathrm{d}z$$

$$\Delta_{25} = \int_{-h/2}^{h/2} \frac{E_2\alpha_1 T_1}{1-v}(T_r-1)(1-\alpha_r)(E_r-1) \times \left(\frac{h-2z}{2h}\right)^{2n} \frac{\Psi_a}{\Psi_b} z\,\mathrm{d}z$$

$$\Delta_{31} = \int_{-h/2}^{h/2} \frac{E_2\alpha_1 T_1}{1-v}(1-2\alpha_r + \alpha_r E_r)\left(\frac{h-2x}{2h}\right)^n z^2\,\mathrm{d}z$$

$$\Delta_{32} = \int_{-h/2}^{h/2} \frac{E_2\alpha_1 T_1}{1-v}(1-\alpha_r) \times (E_r-1)\left(\frac{h-2x}{2h}\right)^{2n} z^2\,\mathrm{d}z$$

$$\Delta_{33} = \int_{-h/2}^{h/2} \frac{E_2\alpha_1 T_1}{1-v}(T_r-1)\alpha_r \frac{\Psi_a}{\Psi_b} z^2\,\mathrm{d}z$$

$$\Delta_{34} = \int_{-h/2}^{h/2} \frac{E_2\alpha_1 T_1}{1-v}(T_r-1)(1-2\alpha_r+\alpha_r E_r) \times \left(\frac{h-2z}{2h}\right)^n \frac{\Psi_a}{\Psi_b} z^2\,\mathrm{d}z$$

$$\Delta_{35} = \int_{-h/2}^{h/2} \frac{E_2\alpha_1 T_1}{1-v}(T_r-1)(1-\alpha_r)(E_r-1) \times \left(\frac{h-2x}{2h}\right)^{2n} \frac{\Psi_a}{\Psi_b} z^2\,\mathrm{d}z$$

$$\alpha_r = \frac{\alpha_2}{\alpha_1}, \qquad E_r = \frac{E_1}{E_2}, \qquad K_r = \frac{K_1}{K_2} \qquad (A.5)$$

$$\Psi_a = \int_{-h/2}^{z} \frac{1}{1+(K_r-1)(\frac{h-2z}{2h})^n}\mathrm{d}z, \qquad \Psi_b = \int_{-h/2}^{h/2} \frac{1}{1+(K_r-1)(\frac{h-2z}{2h})^n}\mathrm{d}z \qquad (A.6)$$

References

1. Ng TY, Lam KY, Liew KM, Reddy JN (2001) Dynamic stability analysis of functionally graded cylindrical shells under periodic axial loading. Int J Solids Struct 38:1295–1309
2. Sofiyev AH, Aksogan O (2004) Bucking of a conical thin shell with variable thickness under a dynamic loading. J Sound Vib 270:903–915
3. Sofiyev AH (2010) Dynamic response of an FGM cylindrical shell under moving loads. Compos Struct 93:58–66
4. Zhu JQ, Chen CQ, Shen YP, Wang SL (2005) Dynamic stability of functionally graded piezoelectric circular cylindrical shells. Mater Lett 59:477–485
5. Cao ZY, Wang HN (2007) Free vibration of FGM cylindrical shells with holes under various boundary conditions. J Sound Vib 306:227–237
6. Hasheminejad SM, Rajabi M (2008) Effect of FGM core on dynamic response of a buried sandwich cylindrical shell in poroelastic soil to harmonic body waves. Int J Press Vessels Piping 85:762–771
7. Matsunaga H (2009) Free vibration and stability of functionally graded circular cylindrical shells according to a 2D higher-order deformation theory. Compos Struct 88:519–531
8. Sheng GG, Wang X (2009) Studies on dynamic behavior of functionally graded cylindrical shells with PZT layers under moving loads. J Sound Vib 323:772–789
9. Pradhan SC, Loy CJ, Lam KY, Reddy JN (2010) Vibration characteristics of functionally graded cylindrical shells under various boundary conditions. Appl Acoust 61:111–129
10. Vel SS (2010) Exact elasticity solution for the vibration of functionally graded anisotropic cylindrical shells. Compos Struct 92:2712–2727
11. Huang HW, Han Q, Wei DM (2011) Buckling of FGM cylindrical shells subjected to pure bending load. Compos Struct 93:2945–2952
12. Dai HL, Dai T, Zheng HY (2012) Stresses distributions in a rotating functionally graded piezoelectric hollow cylinder. Meccanica 47:423–436
13. Asemi K, Akhlaghi M, Salehi M (2012) Dynamic analysis of thick short length FGM cylinders. Meccanica 47:1441–1453
14. Najafov AM, Sofiyev AH, Kuruoglu N (2013) Torsional vibration and stability of functionally graded orthotropic cylindrical shells on elastic foundations. Meccanica 48:829–840
15. Tornabene F, Viola E (2013) Static analysis of functionally graded doubly-curved shells and panels of revolution. Meccanica 48:901–930
16. Jabbari M, Sohrabpour S, Eslami MR (2002) Mechanical and thermal stresses in a functionally graded hollow cylinder due to radially symmetric loads. Int J Press Vessels Piping 79:493–497
17. Jabbari M, Mohazzab AH, Bahtui A, Eslami MR (2007) Analytical solution for three-dimensional stresses in a short length FGM hollow cylinder. Z Angew Math Mech 87:413–429
18. Jabbari M, Bahtui A, Eslami MR (2009) Axisymmetric mechanical and thermal stresses in thick short length FGM cylinders. Int J Press Vessels Piping 86:296–306

19. Haddadpour H, Mahmoudkhani S, Navazi HM (2007) Free vibration analysis of functionally graded cylindrical shells including thermal effects. Thin-Walled Struct 45:591–599
20. Azadi M, Shariyat M (2010) Nonlinear transient transfinite element thermal analysis of thick-walled FGM cylinders with temperature-dependent material properties. Meccanica 45:305–318
21. Dai HL, Zheng HY (2011) Buckling and post-buckling analyses for an axially compressed laminated cylindrical shell of FGM with PFRC in thermal environments. Eur J Mech A, Solids 30:913–923
22. Sladek J, Sladek V, Solek P, Wen PH, Atluri SN (2008) Thermal analysis of Reissner-Mindlin shallow shells with FGM properties by the MLPG. Comput Model Eng Sci 30:77–97
23. Hosseini SM, Sladek J, Sladek V (2011) Meshless Petrov-Galerkin method for coupled thermoelasticity analysis of a functionally graded thick hollow cylinder. Eng Anal Bound Elem 35:827–835
24. Hosseini SM, Shahabian F, Sladek J, Sladek V (2011) Stochastic meshless local Petrov-Galerkin method for thermo-elastic wave propagation analysis in functionally graded thick hollow cylinders. Comput Model Eng Sci 71:39–66
25. Shen HS (2004) Thermal postbuckling behavior of functionally graded cylindrical shells with temperature-dependent properties. Int J Solids Struct 41:1961–1974
26. Shen HS (2007) Thermal postbuckling of shear deformable FGM cylindrical shells with temperature-dependent properties. Mech Adv Mat Struct 14:439–452
27. Shen HS, Noda N (2007) Postbuckling of pressure-loaded FGM hybrid cylindrical shells in thermal environments. Compos Struct 77:546–560
28. Shen HS (2009) Torsional buckling and postbuckling of FGM cylindrical shells in thermal environments. Int J Non-Linear Mech 44:644–657
29. Shen HS (2011) Postbuckling of nanotube-reinforced composite cylindrical shells in thermal environments, part I: axially-loaded shells. Compos Struct 93:2096–2108
30. Shen HS (2011) Postbuckling of nanotube-reinforced composite cylindrical shells in thermal environments, part II: pressure-loaded shells. Compos Struct 93:2496–2503
31. Shen HS (2012) Nonlinear vibration of shear deformable FGM cylindrical shells surrounded by an elastic medium. Compos Struct 94:1144–1154
32. Shen HS, Xiang Y (2012) Nonlinear vibration of nanotube-reinforced composite cylindrical shells in thermal environments. Comput Methods Appl Mech Eng 213–216:196–205
33. Wu LH, Jiang ZQ, Liu J (2005) Thermoelastic stability of functionally graded cylindrical shells. Compos Struct 70:60–68
34. Pelletier JL, Vel SS (2006) An exact solution for the steady-state thermoelastic response of functionally graded orthotropic cylindrical shells. Int J Solids Struct 43:1131–1158
35. Zhang JH, Li SR, Ma LS (2008) Exact solution of thermoelastic bending for functionally graded truncated conical shells. Chin J Theor Appl Mech 40(2):185–193 (In Chinese)
36. Shariyat M (2008) Dynamic buckling of suddenly loaded imperfect hybrid FGM cylindrical shells with temperature-dependent material properties under thermo-electro-mechanical loads. Int J Mech Sci 50:1561–1571
37. Shariyat M (2008) Dynamic thermal buckling of suddenly heated temperature-dependent FGM cylindrical shells, under combined axial compression and external pressure. Int J Solids Struct 45:2598–2612
38. Santos H, Mota Soares CM, Mota Soares CA, Reddy JN (2008) A semi-analytical finite element model for the analysis of cylindrical shells made of functionally graded materials under thermal shock. Compos Struct 86:10–21
39. Zhao X, Liew KM (2009) Geometrically nonlinear analysis of functionally graded shells. Int J Mech Sci 51:131–144
40. Liew KM, Zhao X, Lee YY (2012) Postbuckling responses of functionally graded cylindrical shells under axial compression and thermal loads. Composites, Part B, Eng 43:1621–1630
41. Sheng GG, Wang X (2010) Dynamic characteristics of fluid-conveying functionally graded cylindrical shells under mechanical and thermal loads. Compos Struct 93:162–170
42. Sheng GG, Wang X (2013) An analytical study of the non-linear vibrations of functionally graded cylindrical shells subjected to thermal and axial loads. Compos Struct 97:261–268
43. Huang HW, Han Q (2010) Nonlinear buckling of torsion-loaded functionally graded cylindrical shells in thermal environment. Eur J Mech A, Solids 29:42–48
44. Alibeigloo A (2011) Thermoelastic solution for static deformations of functionally graded cylindrical shell bonded to thin piezoelectric layers. Compos Struct 93:961–972
45. Malekzadeh P, Heydarpour Y (2012) Free vibration analysis of rotating functionally graded cylindrical shells in thermal environment. Compos Struct 94:2971–2981
46. Malekzadeh P, Heydarpour Y (2012) Response of functionally graded cylindrical shells under moving thermo-mechanical loads. Thin-Walled Struct 58:51–66
47. Malekzadeh P, Heydarpour Y, Golbahar Haghighi MR, Vaghefi M (2012) Transient response of rotating laminated functionally graded cylindrical shells in thermal environment. Int J Press Vessels Piping 98:43–56
48. Ma LS, Wang TJ (2003) Nonlinear bending and postbuckling of a functionally graded circular plate under mechanical thermal loadings. Int J Solids Struct 40(13–14):3311–3330